Numerical study of the hydrodynamic performance of a pile-restrained WEC-type floating breakwater

Qiang Chen[1,*], Jun Zang[1], Xuanlie Zhao[2], Dezhi Ning[2]

[1]Research Unit for Water, Environment and Infrastructure Resilience (WEIR), Department of Architecture and Civil Engineering, University of Bath, BA2 7AY, UK

[2]State Key Laboratory of Coastal and Offshore Engineering, Dalian University of Technology, 116024, China

[*]Email: chenqiang913@hotmail.com

HIGHLIGHTS

The hydrodynamic performance of a vertical pile-restrained Wave Energy Converter (WEC) type floating breakwater under regular wave action is simulated using a Particle-In-Cell (PIC) method based numerical model. The numerical results such as the heave motion of the breakwater and the capture width ratio of the integrated system are discussed and compared with experimental measurements.

1 INTRODUCTION

For coastal areas with high tidal range and/or large water depth, floating breakwaters are frequently used as wave-attenuation structures, due to a number of advantages such as the relatively low construction-costs, low environmental impact and flexibility. Meanwhile, as floating breakwaters are similar to the oscillating buoy Wave Energy Converters (WECs) in terms of working conditions, structural characteristics and applied functions, the idea of integrating WECs into floating breakwaters provides a promising way to realize cost-sharing in wave energy technology. A number of pioneering studies show that it is possible to simultaneously realize the function of wave energy utilisation and desired-level wave attenuation for this integrated system (Michailides and Angelides, 2012; He et al., 2013; Ning et al., 2016). Ning et al. (2016) experimentally studied the system of a vertical pile-restrained floating breakwater that is working under the principle of an oscillating buoy WEC. Their results show that with the proper adjustment of power take-off (PTO) damping force, a range can be observed for which the capture width ratio (CWR) of the system can achieve approximately 24%, with the transmission coefficient being lower than 0.50. In this paper, the experimental setup used in Ning et al. (2016) has been numerically studied using a Particle-In-Cell (PIC) method based model. The aims are to first validate the numerical model for simulating the performance of such WEC-type floating breakwater, and then apply the numerical model to further investigations such as the survivability of the integrated system under extreme wave conditions.

The PIC model used in this paper is developed based on that proposed in Chen et al. (2016). The model employs both a set of Lagrangian particles and an Eulerian grid to solve the incompressible Navier-Stokes equations (NSE) for single-phase free-surface flows. The novelty lies in the fact that the linear non-advection terms of the NSE are resolved on the grid, while the nonlinear advection terms are handled using the particles in a Lagrangian manner. This makes the model both efficient and flexible in terms of simulating complex physical problems such as those involving large free-surface deformations (see examples in Kelly et al. (2015) and Chen et al. (2016)). For fluid-structure interaction, the model employs a Cartesian cut cell based two-way strong coupling algorithm and is able to simulate surface-piercing floating bodies of arbitrary configuration and degree of freedom.

2 NUMERICAL MODEL

The PIC model solves the incompressible NSE for single-phase free-surface flows:

$$\nabla \cdot \boldsymbol{u} = 0, \tag{1}$$

$$\frac{\partial \boldsymbol{u}}{\partial t} + (\boldsymbol{u} \cdot \nabla)\boldsymbol{u} = \boldsymbol{f} - \frac{1}{\rho}\nabla p + \nu \nabla^2 \boldsymbol{u}, \tag{2}$$

where, in 2D, $\boldsymbol{u} = [u, w]^T$ is the velocity field; t is time; p is pressure; $\boldsymbol{f}$ = [0.0, -9.81 m/s^2]^T represents the body force due to gravity, and ρ and ν are the density and kinematic viscosity of the fluid, respectively. According to the PIC methodology, both an Eulerian grid and a set of Lagrangian particles are employed to solve the governing equations. In particular, a staggered grid is employed, where pressures are stored at cell centres, whose positions along the x- and z-directions are numbered by indexes i and j, respectively, and velocities are computed at relevant cell edges, whose positions are labelled with half-integer values of the indexes. Four particles are initially seeded in each grid cell in the current 2D model, and cells occupied by the particles are marked as fluid cells. The particles carry the fluid properties such as the mass and momentum, and are used to track the configuration of the fluid body (including the free-surface position) and solve the nonlinear advection term, while the underlying grid is employed solely for computational convenience for solving the non-advection terms.

The solution procedure is divided into two major steps: an Eulerian step and a Lagrangian step. During the Eulerian step the NSE, ignoring the nonlinear advection term, are resolved on the grid using the pressure projection method, where a pressure Poisson equation (PPE) $\Delta t \rho^{-1} \nabla^2 p^{n+1} = \nabla \cdot \tilde{\boldsymbol{u}}$, where $\tilde{\boldsymbol{u}}$ is the tentative velocity at the centres of cell edges after explicitly resolving the body force term and the viscosity term in the momentum equation, is resolved incorporating the boundary conditions. On the structure surface, the following boundary conditions are imposed:

$$\boldsymbol{n} \cdot \boldsymbol{u} = \boldsymbol{n} \cdot \boldsymbol{U}_b \quad \text{and} \quad \boldsymbol{n} \cdot (\Delta t \rho^{-1} \nabla p) = \boldsymbol{n} \cdot (\tilde{\boldsymbol{U}}_b - \boldsymbol{U}_b^{n+1}) \quad \text{on } \partial\Omega_S(\boldsymbol{x}, t), \tag{3}$$

where $\partial\Omega_S$ represents the structure surface; $\boldsymbol{n}$ is the unit outward normal vector of the structure surface; $\tilde{\boldsymbol{U}}_b$ represents a tentative velocity on the structure surface; $\boldsymbol{U}_b^{n+1}$ is the velocity imposed on the structure surface at time step $n+1$. The above boundary conditions are applied using the Cartesian cut cell based fluid-structure coupling algorithm proposed in Ng et al. (2009). Integrating the PPE over a fluid cell, G_{ij}, that is partially occupied by solid structures and evoking the divergence theorem and the above boundary conditions, we obtain:

$$E_{i-\frac{1}{2},j} \cdot \frac{\Delta t(p_{i-1,j}^{n+1} - p_{i,j}^{n+1})}{\rho \Delta x} + E_{i+\frac{1}{2},j} \cdot \frac{\Delta t(p_{i+1,j}^{n+1} - p_{i,j}^{n+1})}{\rho \Delta x} + E_{i,j-\frac{1}{2}} \cdot \frac{\Delta t(p_{i,j-1}^{n+1} - p_{i,j}^{n+1})}{\rho \Delta z} + E_{i,j+\frac{1}{2}} \cdot \frac{\Delta t(p_{i,j+1}^{n+1} - p_{i,j}^{n+1})}{\rho \Delta z}$$
$$= E_{i+\frac{1}{2},j} \cdot \tilde{u}_{i+\frac{1}{2},j} - E_{i-\frac{1}{2},j} \cdot \tilde{u}_{i-\frac{1}{2},j} + E_{i,j+\frac{1}{2}} \cdot \tilde{w}_{i,j+\frac{1}{2}} - E_{i,j-\frac{1}{2}} \cdot \tilde{w}_{i,j-\frac{1}{2}} - \int_{G_{ij} \bigcap \partial\Omega_S} \boldsymbol{n} \cdot \boldsymbol{U}_b^{n+1} \, dl \,, \tag{4}$$

where the subscripts are the space indexes as mentioned above; E represents the fraction of a cell edge that is open-to-water (i.e. not occupied by structures); $\Delta x = \Delta z$ are the grid sizes and dl refers to the line differential. It is noted that for freely movable structures, $\boldsymbol{U}_b^{n+1}$, the velocity imposed on the structure surface, in the last term on the right hand side of Equation 4 is unknown at the time step n. Here, the solution is to transfer the structure velocity to the fluid pressures in cells immediately surrounding the structure:

$$\boldsymbol{U}^{n+1} = \boldsymbol{U}^n + \Delta t M_s^{-1} J p^{n+1} + \Delta t(\boldsymbol{f} + \boldsymbol{F}), \tag{5}$$

where $\boldsymbol{U}^{n+1}$ and $\boldsymbol{U}^n$ are the structure velocities at time step $n+1$ and n, respectively; M_s is the mass matrix of the structure; J is an operator that maps the pressures to net forces on the structure; $\boldsymbol{F}$ represents the external forces due to the PTO system, frictions and moorings. Once the structure velocity is constructed, the velocity integral in Equation 4 can be expressed purely in terms of pressure, leading to a revised PPE. For more details, the reader is referred to Chen et al. (2016).

On the free surface, the boundary condition enforced is:

$$p = 0 \quad \text{on } \zeta(\boldsymbol{x}, t), \tag{6}$$

where $\zeta(\boldsymbol{x}, t)$ represents the free-surface position reconstructed on the grid based on the particle position. This boundary condition is resolved in the same manner as that discussed in Chen et al. (2018), which only changes the coefficient matrix of the linear system of equations of Equation 4.

Once the Eulerian step is completed, a divergence-free velocity field $\boldsymbol{u}^{n+1}$ on the grid is found. In the Lagrangian step, the velocity change (i.e. the acceleration), $\boldsymbol{a}^{n+1} = \boldsymbol{u}^{n+1} - \boldsymbol{u}^n$, on the grid is

interpolated onto the particles to increment the velocity carried by the particles. It is noteworthy that for the purpose of numerical stability, the divergence-free velocity itself on the grid is also interpolated to constitute a small proportion of the final particle velocity (see more details in Chen et al. (2016)). Following Brackbill and Ruppel (1986), the particles, carrying the newly updated velocity field, are then advected through the divergence-free velocity field on the grid, rather than the velocity field they carry. After the particles are advected, one computational cycle of solving the NSE is completed. It is noted that at the beginning of the next computational cycle, the velocity field is mapped from the particles to the grid using a SPH-like kernel interpolation that conserves the mass and momentum. For full details of the PIC model, the reader is referred to Chen (2017).

3 CASE STUDY

The experiments of a WEC-type floating breakwater presented in Ning et al. (2016) are numerically studied using the current PIC model. The experiments were conducted in a wave flume at the State Key Laboratory of Coastal and Offshore Engineering, Dalian University of Technology, China. Figure 1 shows a sketch depicting the setup of the physical model. The integrated system consists of a vertical pile-restrained floating breakwater and a PTO system installed above the breakwater. The breakwater is restricted to heave motion only under wave action, and the heave motion is converted to a rotary motion of the shaft in the PTO system through the meshing engagement of a toothed rack (on the connecting rod) and a gear (fixed at one end of the shaft). A current controller-magnetic powder brake system, which can produce approximate Coulomb damping force, is connected to the other end of the shaft to simulate the power generation system. The breakwater is a rectangular box measuring 0.8 m wide (B), 0.6 m high and 0.78 m long in the transverse direction, with the gap between the breakwater and the flume wall being 0.01 m. The water depth h was fixed at 1.0 m, while the draft of the breakwater changes according to the test cases under consideration. For more details about the experimental setup, the reader is referred to Ning et al. (2016).

A numerical wave tank (NWT) is established for the current numerical simulation. A piston-type wave paddle is employed at the upstream end of the NWT for wave generation and a relaxation zone is used at the downstream end for wave absorption. We note that while the length of the NWT changes for different wave conditions in order to save on CPU cost, the breakwater is always placed at a position approximately 6 wavelengths away from the wave paddle and the relaxation zone is kept at least 2 wavelengths long. The grid size is fixed at 0.02 m and the Courant number is set to 0.5.

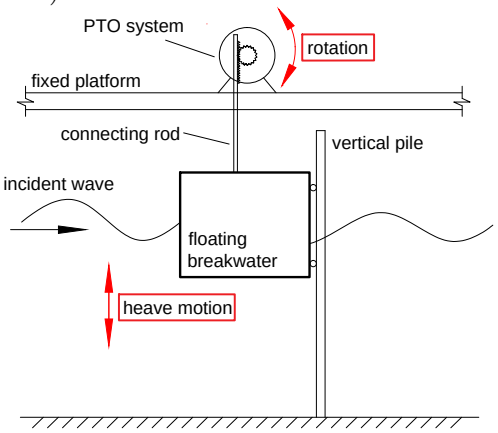

Figure 1: Sketch (side view) of the integrated system.

Regular waves were used in the experiment and the test conditions of the selected test cases for the numerical simulation are given in Table 1, where d is the draft of the breakwater, T is the wave period, L is the wavelength and I is the input current that controls the damping force produced by the magnetic powder brake. The damping forces, corresponding to the input currents, measured in the experiment are shown in Figure 2(b) and are used in the present numerical simulations. For all the selected test cases, the wave height H is fixed at 0.2 m.

Figure 2(a) shows the comparison of the heave motion of the breakwater, non-dimensionalised by the wave height, between the experimental and numerical results for test case 1, where the damping force from the magnetic powder brake is expected to be zero. Figure 2(b) presents the damping forces,

Table 1: Test conditions of the selected test cases.

Test case	d (m)	T (s)	I (A)	B/L
1	0.20	1.16, 1.37, 1.58, 1.79, 2.00, 2.42	0.00	0.38, 0.28, 0.22, 0.18, 0.15, 0.12
2	0.25	1.37, 1.58	0.06–0.30 at 0.06 interval	0.28, 0.22

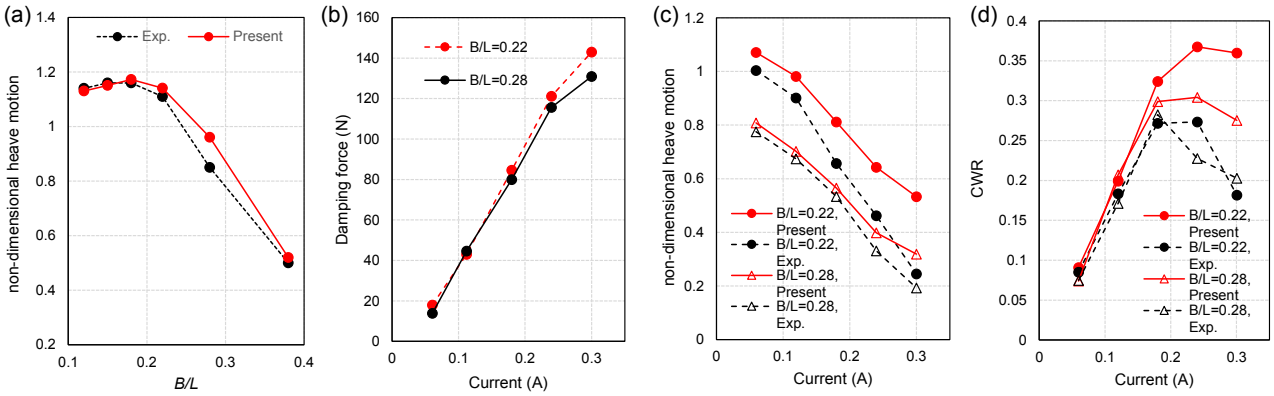

Figure 2: Comparisons for (a) the heave motion of the breakwater for test case 1, (b) the damping forces for test case 2, (c) the heave motion of the breakwater for test case 2 and (d) the corresponding CWR coefficient for test case 2.

corresponding to the input currents, measured in the experiment for test case 2. Figure 2(c) shows the comparison for the non-dimensional heave motion of the breakwater for test case 2, and Figure 2(d) plots the corresponding CWRs (the ratio of captured power and incident wave power). It can be seen from Figure 2(c) and (d) that the numerical results are in general greater than the experimental data, which is possibly due to some friction forces that presented in the experiment are not included in the simulations and the fact that the effect of the rotary motion of the shaft in the PTO system is neglected in the numerical simulations (due to a lack of information from the experiment), which should lower the nature frequency of the integrated system as it may be seen from Figure 2(a) where the peak value of the experimental measurements appears to occur in a lower incident wave frequency than that for the present numerical results. Nevertheless, as seen from Figure 2(d) the PIC model captures the ranges of input damping forces where peak values of the CWR coefficient can be expected.

4 CONCLUSIONS

This abstract presents a numerical study of the hydrodynamic performance of a vertical pile-restrained WEC-type floating breakwater using the PIC numerical model. The PIC model captures the key physical processes of the integrated system under regular wave action. More test cases and results, including the reflection coefficient and transmission coefficient, will also be presented in the Workshop.

ACKNOWLEDGEMENTS

This work is supported by the UK-China joint projects ResIn (EPSRC Grant No. EP/R007519/1) and UK-CIAPP (Grant No. UK-CIAPP/73).

REFERENCES

J. U. Brackbill and H. M. Ruppel. FLIP: A method for adaptively zoned, Particle-In-Cell calculations of fluid flows in two dimensions. *J. Comp. Phys.*, 65:314–343, 1986.

Q. Chen. *Development of a full particle PIC method for simulating nonlinear wave-structure interaction.* PhD thesis, University of Bath, U.K., 2017.

Q. Chen, J. Zang, A. S. Dimakopoulos, D. M. Kelly, and C. J. Williams. A Cartesian cut cell based two-way strong fluid-solid coupling algorithm for 2D floating bodies. *Journal of Fluids and Structures*, 62:252 – 271, 2016.

Q. Chen, J. Zang, D. M. Kelly, and A. S. Dimakopoulos. A 3D parallel particle-in-cell solver for wave interaction with vertical cylinders. *Ocean Engineering*, 147:165 – 180, 2018.

F. He, Z. Huang, and A. W.-K. Law. An experimental study of a floating breakwater with asymmetric pneumatic chambers for wave energy extraction. *Applied Energy*, 106:222 – 231, 2013.

D. M. Kelly, Q. Chen, and J. Zang. PICIN: A Particle–In–Cell solver for incompressible free surface flows with two-way fluid-solid coupling. *SIAM Journal on Scientific Computing*, 37(3):B403–B424, 2015.

C. Michailides and D. C. Angelides. Modeling of energy extraction and behavior of a Flexible Floating Breakwater. *Applied Ocean Research*, 35:77 – 94, 2012.

Y. T. Ng, C. Min, and F. Gibou. An efficient fluid–solid coupling algorithm for single–phase flows. *Journal of Computational Physics*, 228(23):8807–8829, 2009.

D. Ning, X. Zhao, M. Gteman, and H. Kang. Hydrodynamic performance of a pile-restrained WEC-type floating breakwater: An experimental study. *Renewable Energy*, 95:531 – 541, 2016.